

Article

Variable DC-Link Voltage Control of Dual Active Bridge Converter in a Standalone Wind Power Generation System for High-Efficiency Battery-Discharging Operation [†]

Yuto Takayama [‡] and Hiroaki Yamada ^{*‡} 

Graduate School of Sciences and Technology for Innovation, Yamaguchi University,
2-16-1 Tokiwadai, Ube 755-8611, Japan; a003wcu@yamaguchi-u.ac.jp

* Correspondence: hiro-ymd@yamaguchi-u.ac.jp; Tel.: +81-83-685-9471; Fax: +81-83-685-9472

[†] This paper is an extended version of our paper published in The 23rd International Conference on Electrical Machines and Systems (ICEMS2020), Online, 25 November 2020; pp. 1022–1026.

[‡] These authors contributed equally to this work.

Abstract: In this study, we deal with a dual active bridge (DAB) converter-based battery charger in a standalone wind power generation system (WPGS) with a small-scale wind turbine. However, the power conversion efficiency under the low power output in the discharging mode is low. In this paper, we propose variable DC-link voltage control in a standalone WPGS with a DAB converter under a light load. The proposed control can compensate for the shortage of generated power and suppress the peak value of the transformer current. Simulation results demonstrate that the proposed control can decrease the peak value of the transformer current and improve the power conversion efficiency of the DAB converter. An experimental setup was constructed to confirm the basic operation of the variable DC-link voltage control. In addition, a reference DC-link voltage switchover control is proposed to enable a high-efficiency drive under all load ranges. From simulation results, the power loss can be reduced by the switchover control of the reference DC-link voltage.

Keywords: variable DC-link voltage control; dual active bridge converter; standalone wind power-generation system; battery-discharging mode



Citation: Takayama, Y.; Yamada, H. Variable DC-Link Voltage Control of Dual Active Bridge Converter in a Standalone Wind Power Generation System for High-Efficiency Battery-Discharging Operation. *Energies* **2021**, *14*, 6786. <https://doi.org/10.3390/en14206786>

Academic Editor: Michał Kaczmarek

Received: 24 September 2021

Accepted: 14 October 2021

Published: 18 October 2021

Publisher's Note: MDPI stays neutral with regard to jurisdictional claims in published maps and institutional affiliations.



Copyright: © 2021 by the authors. Licensee MDPI, Basel, Switzerland. This article is an open access article distributed under the terms and conditions of the Creative Commons Attribution (CC BY) license (<https://creativecommons.org/licenses/by/4.0/>).

1. Introduction

The Paris Agreement on the reduction of greenhouse gas emissions was adopted in 2015. Renewable energy plays a major role in reducing greenhouse gas emissions. Wind power generation systems (WPGSs) are expected to install in both onshore and offshore areas because WPGSs have great potential to generate large electric power. Therefore, much research has been conducted on WPGSs [1–5]. The expected installed capacity of the WPGSs will reach 2110 GW by 2030 [6]. Standalone WPGSs are often used small-scale WPGSs with a rated power of less than 50 kW. Large-scale WPGSs have been widely installed because the power generation cost is low. On the contrary, small-scale WPGSs are not often installed despite the advantages of ease of installation and maintenance. This is because the generated power is low relative to the cost of small-scale systems. Therefore, the mechanical output of the wind turbine must be maximized for maximizing the generated power. The mechanical output of a wind turbine is decided by the output coefficient which depends on the tip speed ratio (TSR). Thus, the TSR control is widely used to maximize the mechanical output [7].

A previously proposed variable TSR control in a standalone WPGS [8] is shown in Figure 1. The previously proposed WPGS comprises a boost converter, dump load with a buck converter, isolated full-bridge DC/DC converter, and battery. The boost converter controls TSR of the wind turbine. The isolated full-bridge DC/DC converter acts as a battery charger to control the charging current and voltage of the battery. The single-phase

voltage-source inverter (VSI) supplies AC power to the AC load. The buck converter transfers surplus power between the battery and generated power, and the dump load consumes this surplus power to protect the DC-link capacitor C_2 . In [8], we proposed variable TSR control for minimizing the dump load. The reference value of the TSR in the proposed variable TSR control is changed by the surplus power. However, since four converters are required from the generator to the AC load, the power conversion efficiency of the system in Figure 1 is low. Furthermore, since the input voltage of the VSI is low, 48 Vdc at maximum, the output voltage is also low, 25 Vrms. Therefore, in order to apply 100 Vrms to the AC load, a commercial transformer with a turn ratio of 1:4 is required to step up the voltage. As a result, the system does not only become larger and costlier, but also increase the power loss due to the increase in current in the VSI.

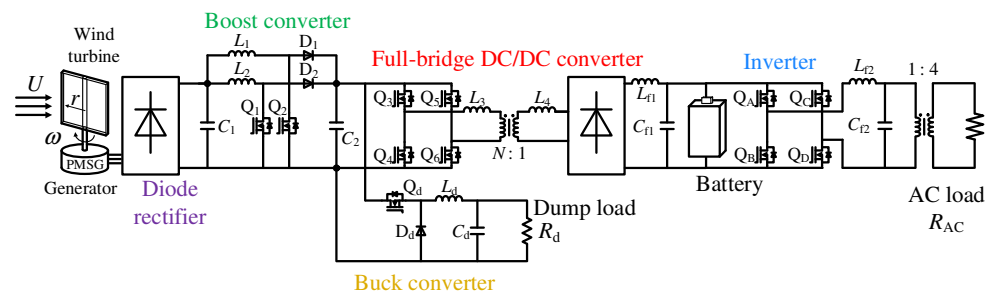


Figure 1. Previously proposed standalone WPGS [8].

Figure 2 shows a standalone WPGS with a pulse width modulation (PWM) rectifier and bidirectional DC-DC converter in [9], and Figure 3 shows a standalone WPGS with a diode rectifier and bidirectional DC-DC converter in [10]. Table 1 lists the comparison of the standalone WPGSs. The system in Figure 2 has two stages of converters between the generator and the AC load, which is less than the system in Figure 1. However, this system requires input current control using a PWM rectifier, which complicates the control. In addition, a cell voltage equalizer is necessary because the batteries need to be connected in series. As a result, the system becomes larger and the control is more complicated. The system in Figure 3 has three stages of converters between the generator and the AC load, which is also less than the system in Figure 1. However, this system requires a commercial transformer in the output side of the VSI due to the low DC-link voltage. As a result, this system leads to larger size, higher cost, and increased power loss of VSI, as in the system in Figure 1.

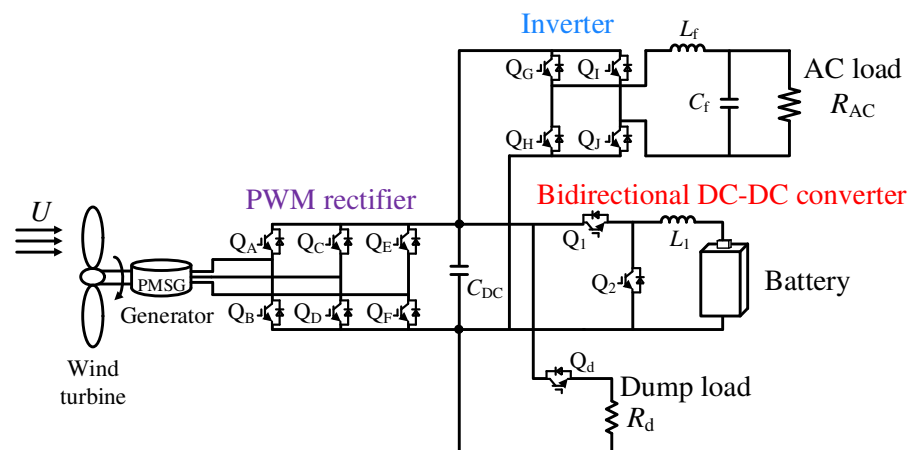


Figure 2. Standalone WPGS with PWM rectifier and non-isolated bidirectional DC-DC converter in [9].

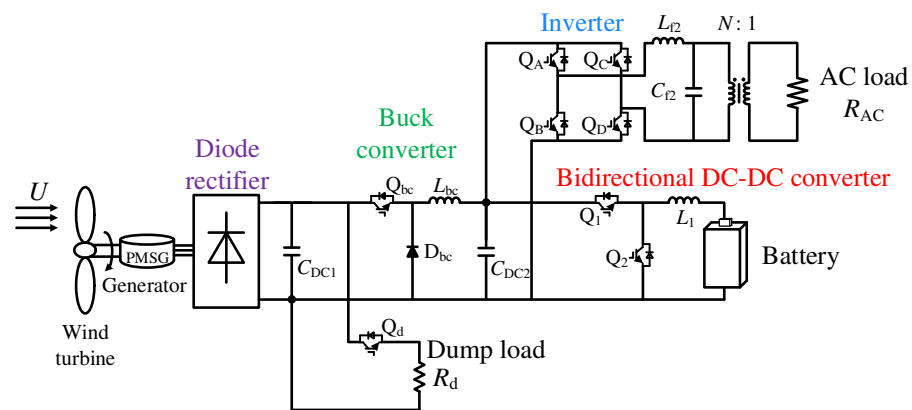


Figure 3. Standalone WPGS with diode rectifier and non-isolated bidirectional DC-DC converter in [10].

Table 1. Comparison of standalone WPGSs.

	Figure 1	Figure 2	Figure 3
Number of stage	4 stages	2 stages	3 stages
Commercial transformer	Necessary	Not necessary	Necessary
Cell voltage equalizer	Not necessary	Necessary	Not necessary

In [11], we proposed a standalone WPGS using a dual active bridge (DAB) converter [12–16]. The DAB converter is one of the isolated bidirectional DC/DC converters and has the advantage of being able to transfer high power. In the proposed system, a DAB converter was used for battery discharging and charging. The power range of a small-scale stand-alone WPGS is up to 50 kW. In this paper, the rated power of a stand-alone WPGS is 500 W for confirming the basic principle of the proposed method in the lab-scale experimental setup. DAB converters have the disadvantage that the DC bias current in the transformer tends to increase when the transferred power changes rapidly. To overcome this problem, several control methods have been proposed [17–19]. On the contrary, the proposed system does not require these countermeasures because the used wind turbine has high inertia and the generated power changes gradually. In [11], the VSI is connected to the common DC-link. Therefore, the power loss can be reduced because the number of converters can be eliminated from the AC load to PMSG and a commercial transformer does not needed. This system can construct without a battery-cell voltage equalizer because the number of the battery in series is small. In [20], we have estimated the power loss of the proposed standalone WPGS. In [21], DAB converter-based battery charger had constructed and tested. Experimental results had demonstrated that the DAB converter can discharge the battery power and the output voltage of the VSI can be maintain constant at about 100 Vrms. In [20,21], primary-side voltage of the DAB converter is constant regardless of the fluctuation of secondary-side voltage. When the voltage ratio of the primary and secondary sides of the DAB converter is larger than the turn ratio of the transformer, the transformer current becomes large, and the power loss of the DAB converter increases. The relationship between the transformer current and power conversion efficiency must be investigated to achieve a high-efficiency WPGS.

In this paper, we propose variable DC-link voltage control in a standalone WPGS with a DAB converter in the battery-discharging mode. The reference DC-link voltage depends on the battery voltage to reduce the peak transformer current. Therefore, the proposed control cannot only compensate for shortage of the generated power but also maintain the voltage ratio between the primary and secondary sides of the DAB converter to the same value as the turn ratio of the transformer. Consequently, the peak value of the transformer current is suppressed and the power conversion efficiency of the DAB converter

is improved. In Section 2, we show the system configuration of a standalone WPGS with a DAB converter, and state variable modulation index control of the VSI. In Section 3, we describe the proposed variable DC-link voltage control in a standalone WPGS with a DAB converter in the battery-discharging mode. Simulation results demonstrate that our proposed control can decrease the peak value of the transformer current and improve the power conversion efficiency of the DAB converter. In Section 4, an experimental setup was constructed to confirm the basic operation of the proposed control system. In Section 5, we propose a reference DC-link voltage switchover control to achieve a high-efficiency WPGS. In the proposed reference DC-link voltage switchover control, variable DC-link voltage control is used in the low-output power region. If the output power increases, the reference DC-link voltage is switched over to a constant value. Simulation results demonstrate that the proposed reference DC-link voltage switchover control is useful for achieving a high-efficiency standalone WPGS.

2. Standalone WPGS with DAB Converter

2.1. System Configuration

Figure 4 shows a standalone WPGS with a DAB converter. The WPGS comprises of a boost converter, single-phase VSI, DAB converter, battery, and dump load. The permanent magnet synchronous generator (PMSG) is used as a generator. The TSR is controlled by the boost chopper for maximizing the mechanical output [8]. The VSI is used to supply AC voltage to AC loads such as AC servo motors and street lights. The modulation index of the VSI is variable to maintain the output voltage of the VSI because the DC-link voltage fluctuates depending on the power generated by the wind turbine. The DAB converter controls the battery current, voltage, and DC-link voltage by the battery. The DC-link side of the DAB converter is defined as the primary side, and the battery side is defined as the secondary side. The direction from the primary side to the secondary side is the charging direction, and the direction from the secondary side to the primary side is the discharging direction. The transferred power is defined as positive in the discharging direction.

As is well-known, the transferred power from the secondary side to the primary side p_{bat} is given as

$$p_{\text{bat}} = \frac{Nv_{\text{DC}}v_{\text{bat}}}{2\pi f_{\text{sw}}l} \phi \left(1 - \frac{|\phi|}{\pi} \right), \quad (1)$$

where N is the turn ratio of the transformer, v_{DC} and v_{bat} are the primary and secondary-side voltages of the DAB converter, respectively, f_{sw} is the switching frequency of the DAB converter, l is the leakage inductance of the transformer, and ϕ is the phase difference between the primary and secondary sides of the DAB converter. The dump load consumes surplus power between the generated power and the load-side power to protect the DC-link capacitor.

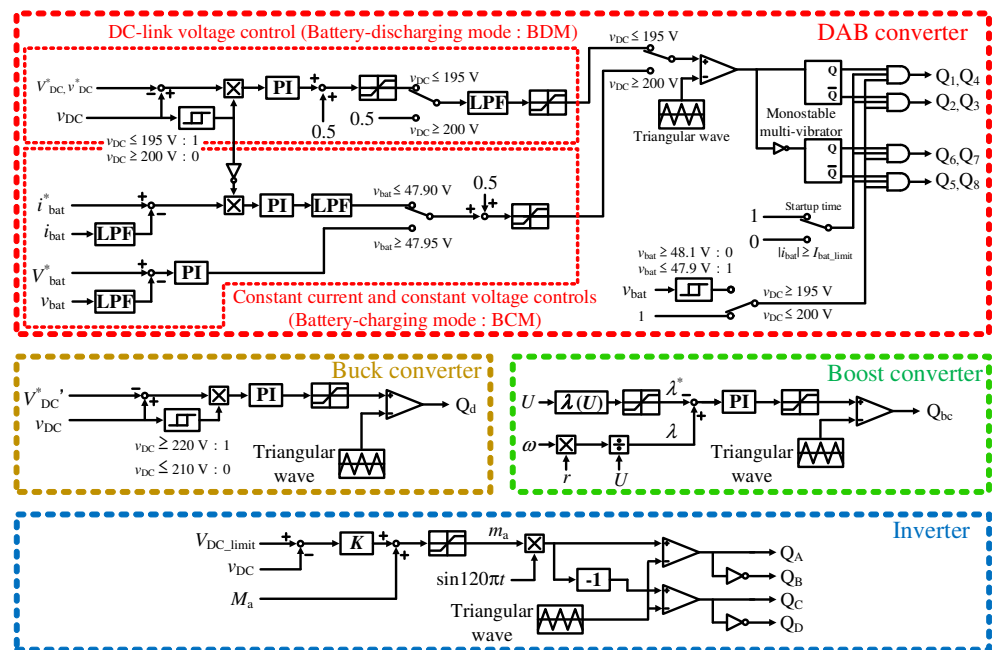
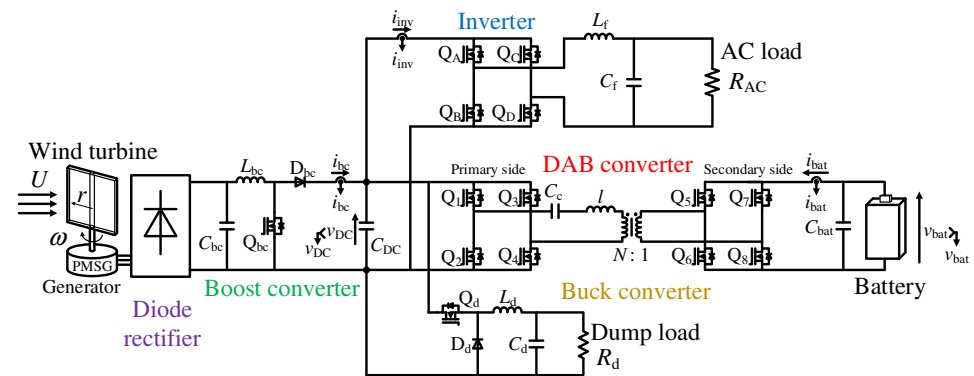


Figure 4. Standalone WPGS with a DAB converter.

2.2. Variable Modulation Index Control of VSI

The DC-link voltage changes owing to the generated power and battery voltage fluctuation. The supply voltage must be maintained within 101 ± 6 Vrms which is defined the Electricity Business Act in Japan [22]. The modulation index is needed to change for keeping the effective value of the VSI due to the DC-link voltage fluctuation. The output voltage v_{AC} of the VSI is given as

$$\begin{aligned}
 v_{AC} &= m_a v_{DC} \sin 120\pi t, \\
 &= \{0.678 + 0.00353(220 - v_{DC})\} v_{DC} \sin 120\pi t,
 \end{aligned}
 \tag{2}$$

where m_a is the modulation index, and v_{DC} is the input voltage of the VSI. The error by subtracting v_{DC} from the limited value is amplified the gain $K = 0.00353$. The reference modulation index m_a is obtained by adding the amplified value and base modulation index value of 0.678. Then, the reference output voltage is multiplied by the sinusoidal wave with frequency of 60 Hz by m_a . The unipolar PWM technique was applied for generating the switching signals. From Equation (2), where v_{DC} is 165 V and the amplitude of v_{AC} is 144 V. In contrast, when v_{DC} is 220 V, the amplitude of v_{AC} is 149 V. Actually, the amplitude of v_{AC} becomes 141 V under the influence of a dead time $0.4 \mu s$. Thus, the RMS value of v_{DC} is almost constant at approximately 100 Vrms.

3. Proposed Variable DC-Link Voltage Control

3.1. Conventional Constant DC-Link Voltage Control

In this section, the conventional constant DC-link voltage control is described. The initial mode of the system is the battery-discharging mode. In [20], the reference voltage V_{DC}^* was set to 194.4. The DC-link voltage is controlled by the DAB converter in the battery-discharging mode.

In the conventional constant DC-link voltage control, the primary-side voltage of the DAB converter is kept constant regardless of the battery voltage fluctuation. Figure 5 shows a simplified circuit configuration of the DAB converter in the battery-discharging mode without the power generated by the wind turbine. In Figure 5, the variable voltage sources v_{DC} and v_{bat} are connected to the primary and secondary sides of the DAB converter, respectively, l is the leakage inductance of the transformer. Figure 6 shows the waveforms of the transformer voltage and current when v_{DC} is larger than Nv_{bat} . The slope of the secondary-side current di_{tr2}/dt is expressed as

$$\frac{di_{tr2}}{dt} = \frac{N}{l}(Nv_{tr2} - v_{tr1}), \tag{3}$$

where the transformer is ideal except for the leakage inductance l .

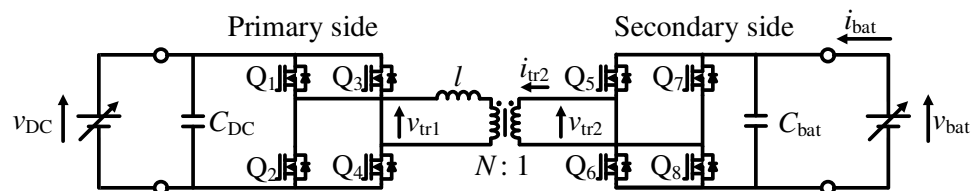


Figure 5. Simplified circuit configuration of DAB converter in battery-discharging mode without power generated by wind turbine.

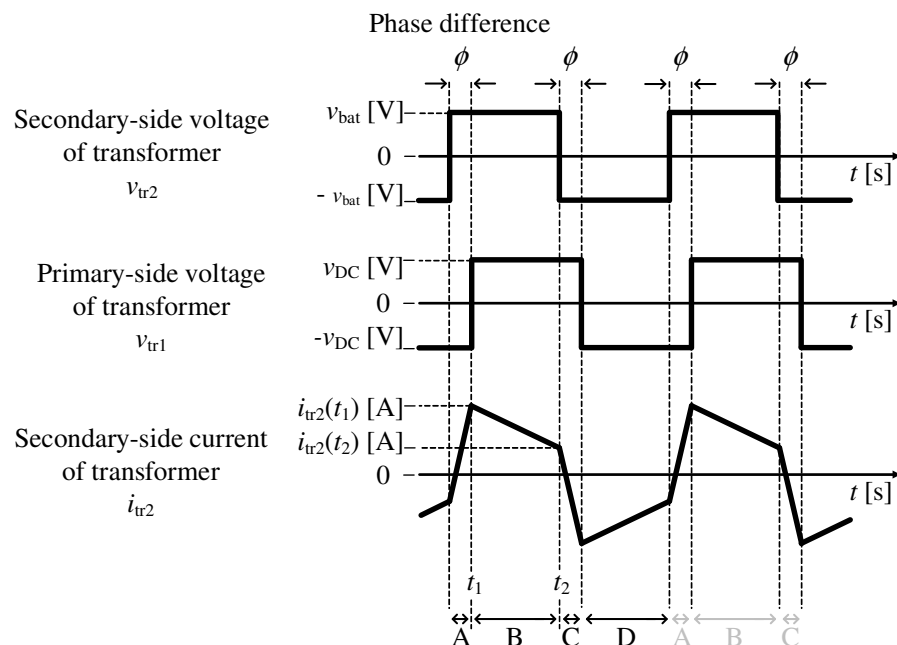


Figure 6. Waveforms of transformer voltage and current when v_{DC} is larger than Nv_{bat} .

From Equation (3), where the voltage ratio of the primary and secondary sides is the same as the turn ratio of the transformer, di_{tr2}/dt in sections B and D is 0. On the contrary, when the voltage ratio and transformer turn ratio are very different, the slope of i_{tr2} increases, and the peak value of i_{tr2} increases. The peak value was $i_{tr2}(t_1)$ when

$v_{DC} < N v_{bat}$. However, when $v_{DC} > N v_{bat}$, the peak value is $i_{tr2}(t_2)$. $i_{tr2}(t_1)$ and $i_{tr2}(t_2)$ are expressed as follows:

$$i_{tr2}(t_1) = \frac{N(2\phi - \pi)v_{DC} + \pi N^2 v_{bat}}{4\pi f_{sw} l}. \quad (4)$$

$$i_{tr2}(t_2) = \frac{N\pi v_{DC} + (2\phi - \pi)N^2 v_{bat}}{4\pi f_{sw} l}. \quad (5)$$

Moreover, when $v_{DC} \neq N v_{bat}$, the RMS value of the transformer current I_{tr2} also increases, as expressed by

$$I_{tr2} = \frac{N\sqrt{N} v_{DC} v_{bat}}{2\pi f_{sw} l} \sqrt{-\frac{2}{3\pi} \phi^3 + \phi^2 + \frac{\pi^2}{12} \frac{(v_{DC} - N v_{bat})^2}{N v_{DC} v_{bat}}}. \quad (6)$$

The larger the peak and RMS values of the transformer current, the larger the following losses of the DAB converter.

- Conduction loss of switch and conducting wire
- Copper loss of transformer
- Loss by equivalent series resistor of capacitor
- Loss by back power flow
- Switching loss increased by failure of zero voltage switching (ZVS)

3.2. Proposed Variable DC-Link Voltage Control

To improve the power conversion efficiency of the DAB converter, we propose a variable DC-link voltage control. From Section 3.1, the v_{DC} should be controlled to maintain

$$v_{DC} = N v_{bat}. \quad (7)$$

v_{tr1} in Section B of Figure 6 becomes $N v_{bat}$, and the peak value of the transformer current is suppressed. As the voltage ratio of the primary and secondary sides is always the same as the turn ratio of the transformer, ZVS can be performed for all phase difference ranges. In addition, as the transformer current decreases, each loss becomes smaller. As a result, the power conversion efficiency of the DAB converter increased.

Here, Equation (7) needs to be added to the compensation value when using an actual transformer. Figure 7 shows the equivalent circuit of the DAB converter in Section B of Figure 6. In Figure 7, \dot{Z}_1 denotes the synthetic impedance of primary-side winding resistance and leakage inductance, \dot{Z}_2 is the synthetic impedance of secondary-side winding resistance r_2 and leakage inductance l_2 , \dot{Z}_0 is exciting impedance. From the superposition theorem, the secondary-side current of the transformer i_{tr2} is expressed as

$$i_{tr2} = \frac{(N^2 \dot{Z}_0 + \dot{Z}_1) v_{bat} - N \dot{Z}_0 v_{DC}}{\dot{Z}_1 \dot{Z}_2 + N^2 \dot{Z}_2 \dot{Z}_0 + \dot{Z}_0 \dot{Z}_1}. \quad (8)$$

From Faraday's law of induction, the slope of the secondary-side current di_{tr2}/dt can be expressed as

$$\begin{aligned} \frac{di_{tr2}}{dt} &= \frac{1}{l_2} v_{l2}, \\ &= \frac{1}{l_2} \left(v_{bat} - r_2 i_{tr2} - \frac{\dot{Z}_0}{\frac{1}{N^2} \dot{Z}_1 + \dot{Z}_0} \frac{1}{N} v_{DC} \right), \\ &= \frac{\left(1 - \frac{N^2 r_2 \dot{Z}_0 + r_2 \dot{Z}_1}{\dot{Z}_1 \dot{Z}_2 + N^2 \dot{Z}_2 \dot{Z}_0 + \dot{Z}_0 \dot{Z}_1} \right) v_{bat} - \left(\frac{N \dot{Z}_0}{\dot{Z}_1 + N^2 \dot{Z}_0} - \frac{N r_2 \dot{Z}_0}{\dot{Z}_1 \dot{Z}_2 + N^2 \dot{Z}_2 \dot{Z}_0 + \dot{Z}_0 \dot{Z}_1} \right) v_{DC}}{l_2}. \end{aligned} \quad (9)$$

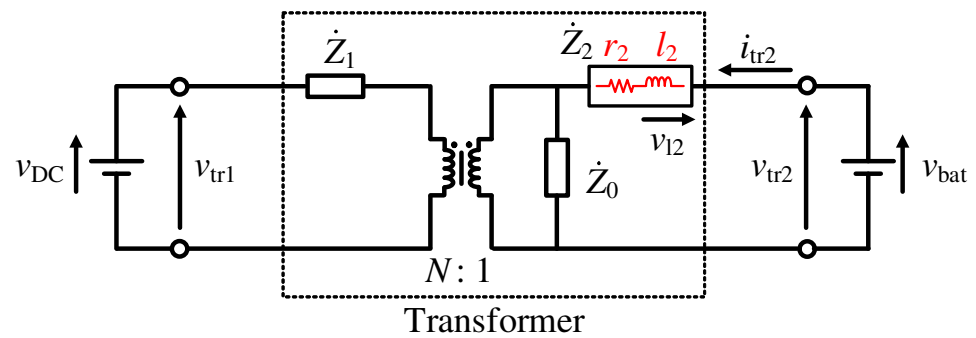


Figure 7. Equivalent circuit of DAB converter in Section B of Figure 6.

Therefore, di_{tr2}/dt does not become zero even if v_{DC}^* satisfies Equation (7). From Equation (10), the condition that $di_{tr2}/dt = 0$ is given by

$$v_{DC} = \frac{(N^2\dot{Z}_0 + \dot{Z}_1)(\dot{Z}_1\dot{Z}_2 + N^2\dot{Z}_2\dot{Z}_0 + \dot{Z}_0\dot{Z}_1) - r_2(N^2\dot{Z}_0 + \dot{Z}_1)^2}{N\dot{Z}_0(\dot{Z}_1\dot{Z}_2 + N^2\dot{Z}_2\dot{Z}_0 + \dot{Z}_0\dot{Z}_1) - Nr_2\dot{Z}_0(N^2\dot{Z}_0 + \dot{Z}_1)} v_{bat}. \quad (10)$$

Here, r_2 is set to 0 for simple calculation and v_{DC} is given by

$$\begin{aligned} v_{DC} &= \frac{(N^2\dot{Z}_0 + \dot{Z}_1)(\dot{Z}_1\dot{Z}_2 + N^2\dot{Z}_2\dot{Z}_0 + \dot{Z}_0\dot{Z}_1)}{N\dot{Z}_0(\dot{Z}_1\dot{Z}_2 + N^2\dot{Z}_2\dot{Z}_0 + \dot{Z}_0\dot{Z}_1)} v_{bat}, \\ &= \left(N + \frac{\dot{Z}_1}{N\dot{Z}_0} \right) v_{bat}. \end{aligned} \quad (11)$$

Therefore, reference value of variable DC-link voltage control v_{DC}^* is set to

$$v_{DC}^* = \left(N + \frac{|\dot{Z}_1|}{N|\dot{Z}_0|} \right) v_{bat}. \quad (12)$$

Equation (12) does not consider the voltage drops generated by switches Q_1 – Q_8 and winding resistance r_2 . Adjusting the actual compensation value while conducting computer simulations and experiments is necessary. In this study, the compensation value is set to $0.05 v_{bat}$ and v_{DC}^* is given as

$$v_{DC}^* = (N + 0.05) v_{bat}. \quad (13)$$

The peak value of the transformer current is suppressed by satisfying Equation (13). However, the output current of the DAB converter increases because v_{DC}^* at the variable DC-link voltage control is lower than V_{DC}^* at a constant DC-link voltage control. As a result, the power conversion efficiency decreases under heavy load conditions.

3.3. Comparison between Each Control Method

All simulations were performed using the PLECS to confirm the peak value of the transformer current and the power conversion efficiency for each control method. Figure 8 shows the circuit configuration of the DAB converter-based WPGS in the battery-discharging mode. In this study, it was assumed that the generated power was zero to confirm the battery-discharging mode. Table 2 lists the circuit constants shown in Figure 8.

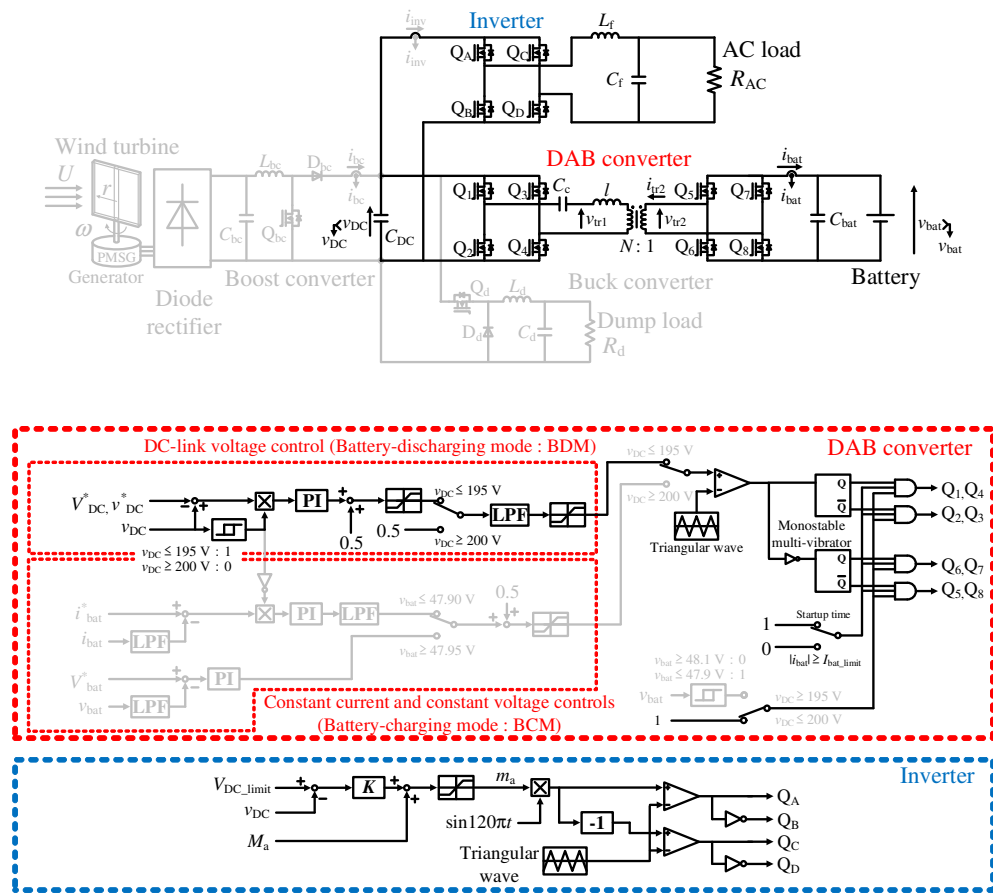


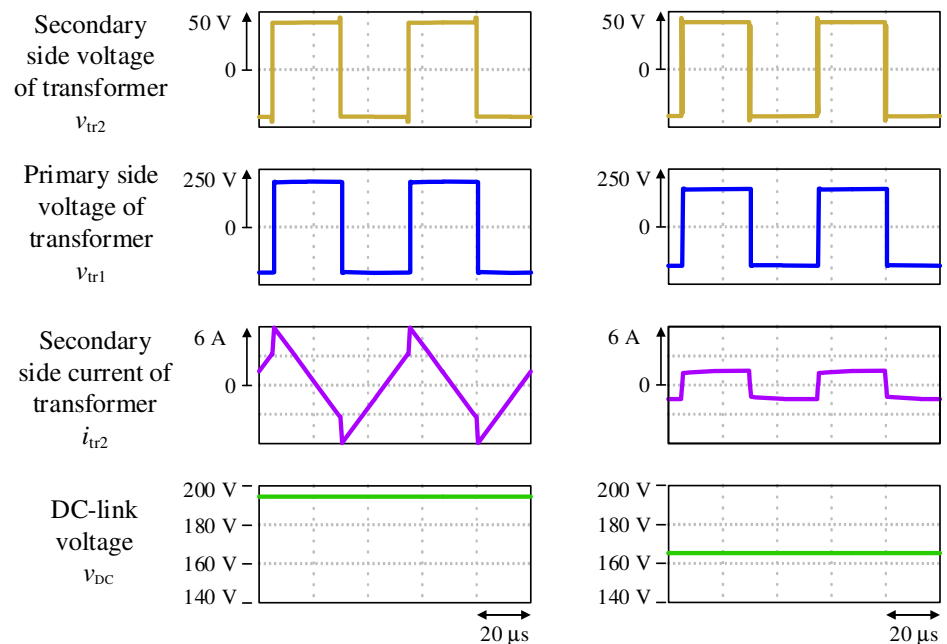
Figure 8. Circuit configuration of DAB converter-based WPGS in battery-discharging mode.

Four lead-acid batteries with a nominal voltage of 12.0 V are connected to the secondary side of the DAB converter in series. Discharge cutoff voltage is 40.8 V and fully charged voltage is 48.0 V. Rated power of the DAB converter is designed to be 500 W. The AC load R_{AC} was varied from 200 Ω to 20 Ω so that the transferred power p_{bat} changed from 10% (50 W) to 100% (500 W) of the rated power.

Figure 9 shows the simulation waveforms of the DAB converter when $p_{bat} = 50$ W and $v_{bat} = 40.8$ V. v_{tr2} and v_{tr1} are the secondary- and primary-side voltages of the transformer, i_{tr2} is the secondary-side current of the transformer, v_{DC} is the DC-link voltage. In the constant DC-link voltage control, v_{DC} agrees with the reference value of 194 V, and the peak value of i_{tr2} is 5.93 A. In the variable DC-link voltage control, v_{DC} agrees with the reference value of 165 V. Because the output voltage of the DAB converter v_{DC} is lower than that of the constant DC-link voltage control, the output current increases. However, i_{tr2} has a trapezoidal wave shape with a peak value of 1.55 A. The peak value of i_{tr2} was reduced by 73.9% when the p_{bat} was 10% of the rated power. Figure 10 shows the reduction rate of the peak value of the transformer current by variable DC-link voltage control. The horizontal axis is the battery voltage v_{bat} , and the vertical axis is the reduction rate of the peak value of the secondary-side current of the transformer i_{tr2} by the variable DC-link voltage control ΔI . ΔI becomes larger under light load. On the contrary, the heavier the load, the smaller the ΔI , and it is almost zero when the load is 100%. This is because the effect of a larger output current is noticeable. When $v_{bat} = 48$ V, ΔI is 0 because the reference values of each control are the same. Thus, the peak value of i_{tr2} at the variable DC-link voltage control can be less than or equal to that at a constant DC-link voltage control under all conditions.

Table 2. circuit constants shown in Figure 8.

Item	Symbol	Value
Battery voltage	v_{bat}	40.8 V to 48.0 V
Resistance load	R_{AC}	20 Ω to 200 Ω
Filter inductor	L_f	984 μH
Smoothing capacitor	C_{bat}	4700 μF
DC-link capacitor	C_{DC}	4700 μF
Coupling capacitor	C_c	3 μF
Filter capacitor	C_f	6.52 μF
Turn ratio of transformer	$N : 1$	4:1
Leakage inductance of transformer	l	320 μH
Winding resistance of transformer		123 m Ω
Exciting conductance of transformer		1.38 mS
Exciting susceptance of transformer		8.13 mS
Switching frequency	f_{sw}	20.0 kHz
Cut-off frequency of LC filter	f_c	1.99 kHz
Dead time		0.4 μs



(a) Constant DC-link voltage control (b) Variable DC-link voltage control

Figure 9. Simulation waveforms of DAB converter when $p_{\text{bat}} = 50 \text{ W}$ (10%) and $v_{\text{bat}} = 40.8 \text{ V}$.

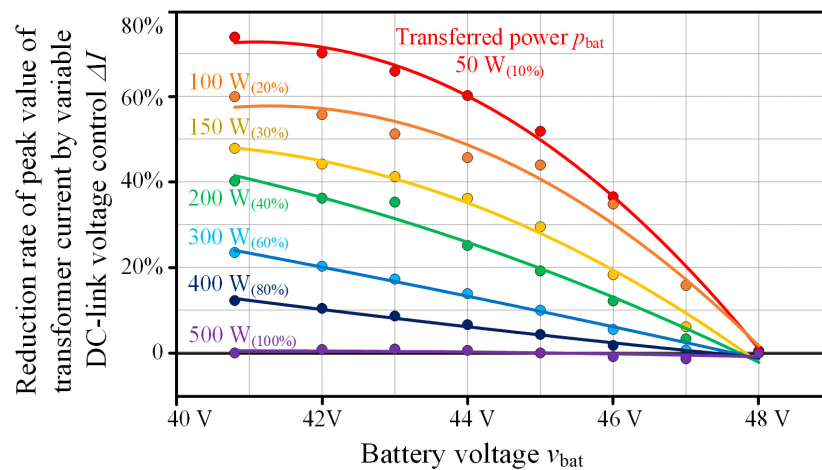


Figure 10. Reduction rate of peak value of transformer current by variable DC-link voltage control.

Figure 11 shows the power conversion efficiency between variable and constant DC-link voltage controls. The horizontal axis represents the battery voltage v_{bat} , and the vertical-axis represents the power conversion efficiency between the variable and constant DC-link voltage controls η . The efficiency is calculated by the difference between the input and output power of the DAB converter, and the switching loss was not considered. Figure 12 shows the power conversion efficiency difference between each control. The horizontal axis is the battery voltage v_{bat} , and the vertical axis is the power conversion efficiency difference between the variable and constant DC-link voltage controls $\Delta\eta$. $\Delta\eta > 0$ means that the variable DC-link voltage control is highly efficient, and $\Delta\eta < 0$ means that the constant DC-link voltage control is highly efficient. When $p_{bat} = 50\text{ W}$, $v_{bat} = 40.8\text{ V}$, and $\Delta\eta$ is 1.12%, which is the maximum with regard to the effect of suppressing the peak value of the transformer current by the variable DC-link voltage control. On the contrary, when $p_{bat} = 500\text{ W}$, $v_{bat} = 40.8\text{ V}$, $\Delta\eta$ is -0.822% , which is the minimum with regard to the effect of increasing the output current of the DAB converter by the variable DC-link voltage control. When $v_{bat} = 48\text{ V}$, $\Delta\eta$ is zero because the reference values of each control are the same. As shown in Figure 12, the variable DC-link voltage control is highly efficient under the transferred power below 150 W (30%), and the constant DC-link voltage control is highly efficient under the transferred power above 200 W (40%). From the above, it is confirmed that the variable DC-link voltage control is effective for improving the power conversion efficiency under a light load. However, these simulations did not consider the switching loss. ZVS is possible with variable DC-link voltage control even under light load where ZVS fails with the constant DC-link voltage control. Therefore, actual $\Delta\eta$ may improve from the values shown in Figure 12.

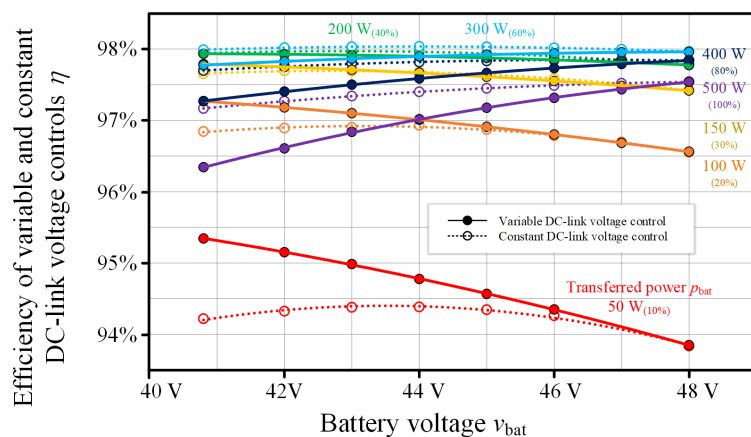


Figure 11. Power conversion efficiency between variable and constant DC-link voltage controls.

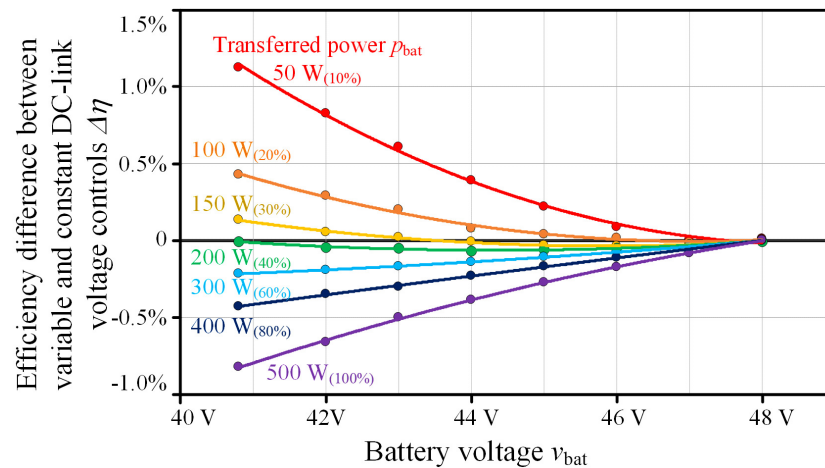


Figure 12. Power conversion efficiency difference between variable and constant DC-link voltage controls.

4. Experimental Verification of Variable DC-Link Voltage Control

An experimental setup was constructed and tested to confirm the basic operation of the proposed variable DC-link voltage control. Figure 13 shows the experimental setup in the battery-discharging mode. Figure 14 shows a block diagram of the experimental setup. The circuit constants are the same as those in Table 2. A DC power supply was used which is assumed as a battery. SiC-MOSFETs (SCT3022AL) were used in all switches. TMS320C28345 which is a digital signal processor (DSP) is used to calculate the reference phase shift angle of the DAB converter and generate the gate signals for the VSI. The gate signals for the DAB converter were generated by the Basys2 with Spartan-3E which is a field programmable gate array (FPGA). Figure 15 shows the transformer used in the DAB converter. The core material was FINEMET FT-3M, a nanocrystalline soft magnetic material from Hitachi Metals, Ltd. The shape of the core was SC-10 of Nihon Cut Core Trans Co., Ltd which is located in Saitama, Japan.

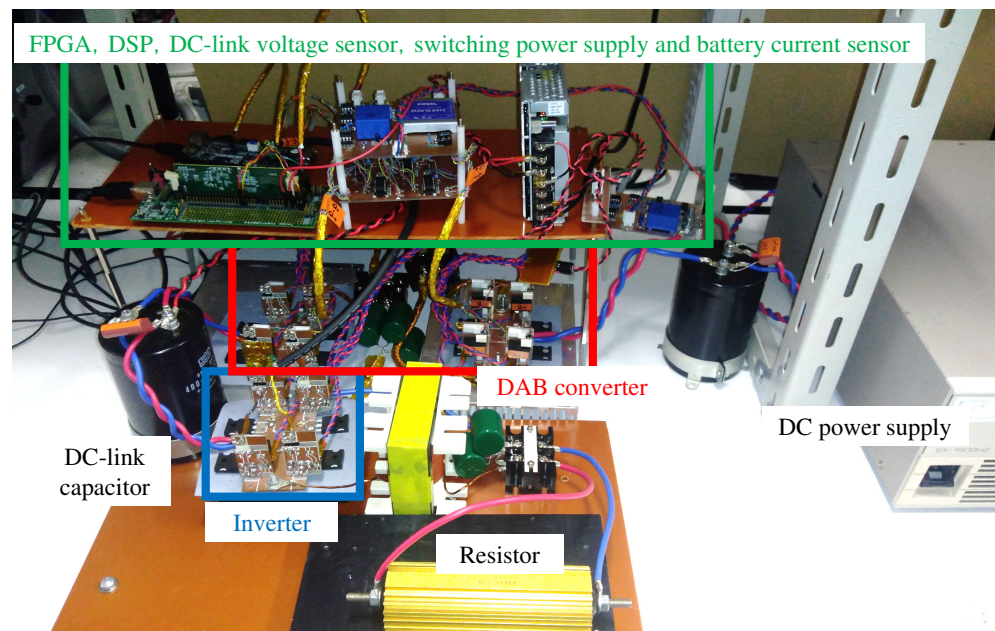


Figure 13. Experimental setup of DAB converter-based WPGS in battery-discharging mode.

Figure 16 shows experimental results of the DAB converter when $v_{bat} = 40.8$ V. v_{tr2} and v_{tr1} are the secondary- and primary-side voltages of the transformer. i_{tr1} is the primary-side current of the transformer. v_{DC} is the DC-link voltage. The phase difference between the two bridges ϕ was 8.64° and the DC-link voltage v_{DC} was 163 V. The error between

v_{DC} and v_{DC}^* was 1.36%. Figure 17 shows the experimental results of the DAB converter when $v_{bat} = 48.0$ V. ϕ was 6.91° and v_{DC} rose to 192 V. The error between v_{DC} and v_{DC}^* was 1.23%. Figures 16 and 17 show that i_{tr2} is always trapezoidal shaped owing to the proposed variable DC-link voltage control as in the simulation results.

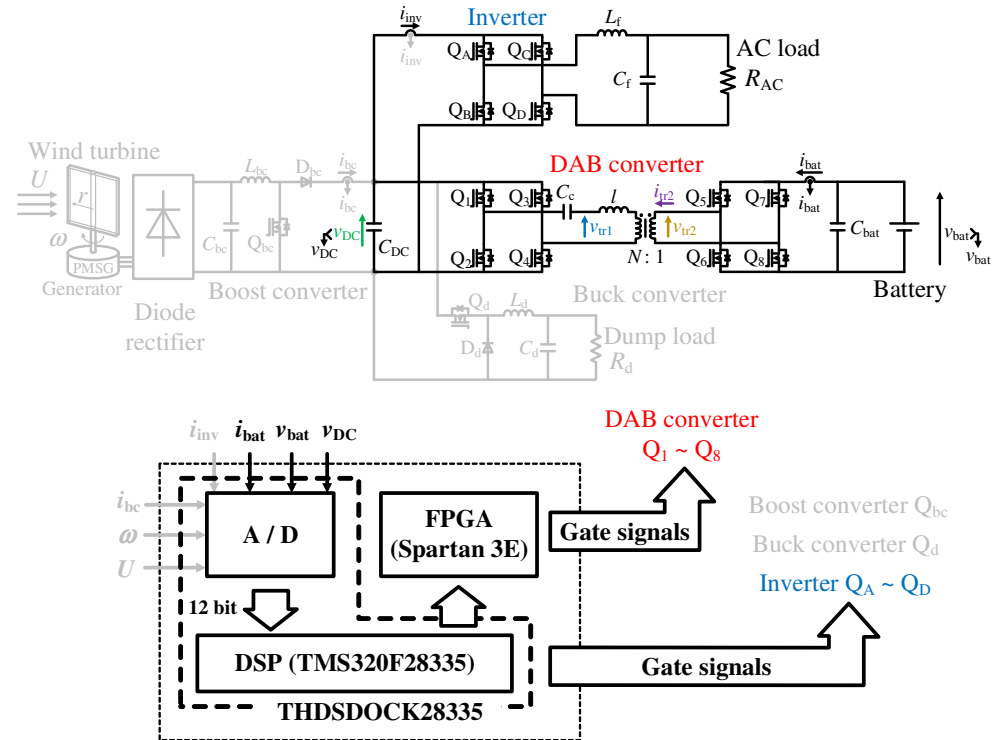


Figure 14. Block diagram of experimental setup.



Figure 15. Transformer used in DAB converter.

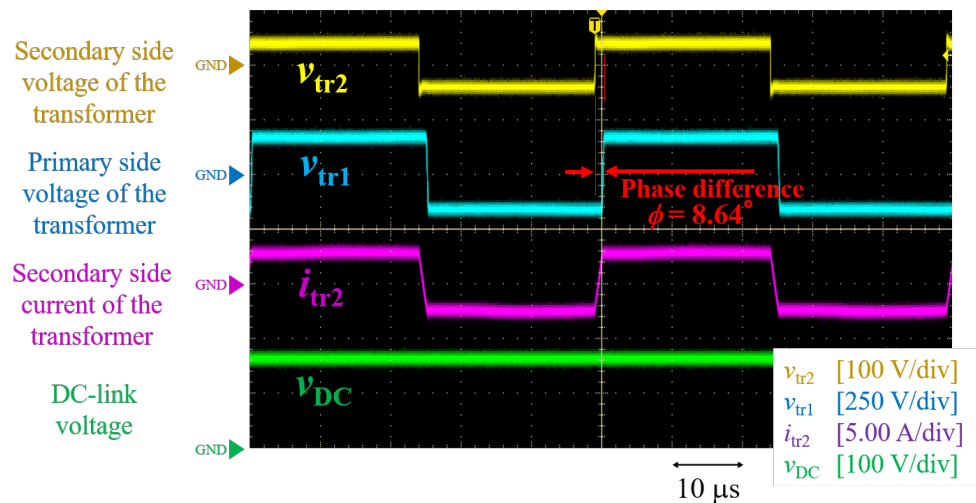


Figure 16. Experimental results of DAB converter when $v_{bat} = 40.8$ V.

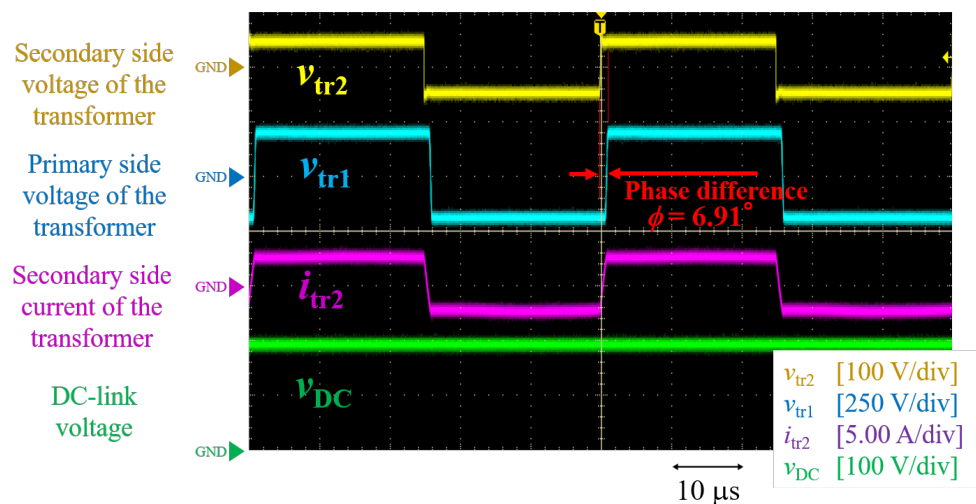


Figure 17. Experimental results of the DAB converter when $v_{bat} = 48.0$ V.

5. Proposed Reference DC-link Voltage Switchover Control

Variable DC-link voltage control is effective at improving the power conversion efficiency under a light load. On the contrary, constant DC-link voltage control is more efficient under heavy loads. Therefore, a high-efficiency drive is possible under all load ranges owing to switching over the DC-link voltage reference value according to the transferred power of the DAB converter. Figure 18 shows the control block of the reference DC-link voltage generation with the proposed reference DC-link voltage switchover control. The transferred power p_{bat} was calculated using $v_{bat}i_{bat}$. The reference value is initially set to the variable DC-link voltage reference value $4.05v_{bat}^*$ and switched over to the constant DC-link voltage reference value 194.4 V when p_{bat} exceeds 200 W. When p_{bat} falls below 150 W, the reference value returns to the variable DC-link voltage reference value $4.05v_{bat}^*$. In addition, the reference value is changed slowly when the reference value is switched over. A computer simulation is implemented using PLECS to confirm the practicability of the proposed reference DC-link voltage switchover control. The simulation circuit is the same as in Figure 8, and the circuit constants are the same as those in Table 2. The battery voltage v_{bat} is fixed at 40.8 V. Therefore, the reference value at the variable DC-link voltage control is constant at 165 V. The AC load R_{AC} was varied between 100 Ω and 33.3 Ω to change the transferred power p_{bat} between 100 W and 300 W.

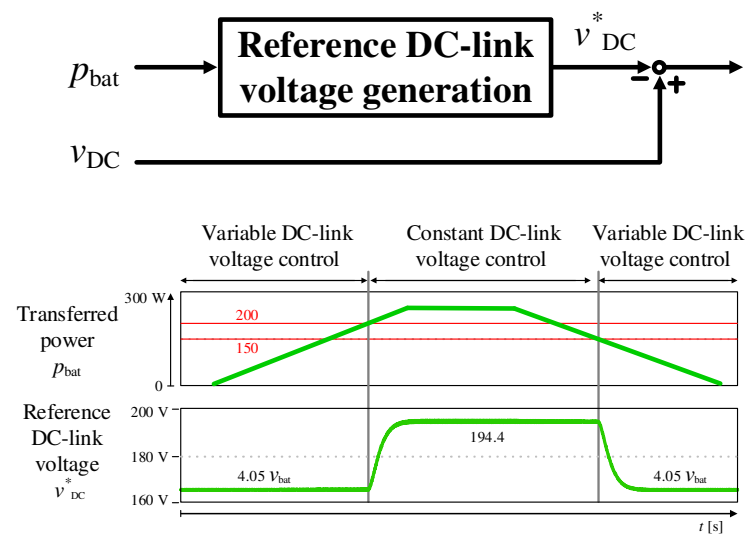


Figure 18. Control block of reference DC-link voltage generation with proposed reference DC-link voltage switchover control.

Figure 19 shows the simulation results for the reference DC-link voltage switchover control. The reference value of the DC-link voltage is switched over according to the p_{bat} . Figure 19 shows that the DC-link voltage v_{DC} changes slowly when the reference value is switched over. At this time, the p_{bat} changes due to charging or discharging of the DC-link capacitor C_{DC} . However, there was no significant effect on v_{tr2} , v_{tr1} , and i_{tr2} , and their values changed slowly. As a result, the proposed reference DC-link voltage switchover control is confirmed to operate properly.

The efficiency difference between variable and constant DC-link voltage controls tends to be the almost same even when the rated power of the DAB converter is changed. When the rated power is 50 kW, the transferred power is 10% of the rated power (5 kW) and battery voltage is 40.8 V, the efficiency difference is about 1.12% as well. In this case, the power loss difference is 56.0 W. Assuming that the battery discharges 12 h a day, 245 kWh of electricity will be saved in one year. This is equivalent to a reduction of 6132 Japanese yen which is about 54.3 USD per year, assuming that the electricity rate is 25 Japanese yen which is about 0.22 USD /kWh. On the contrary, when the transferred power is 100% of the rated power 500 kW, the efficiency difference between variable and constant DC-link voltage controls is about -0.822% . This corresponds to an increase of 45,007 Japanese yen which is about 399 USD per year when calculated in the same way. However, the reference DC-link voltage switchover control acts as the constant DC-link voltage control under heavy loads. Thus, the loss difference between the conventional DC-link voltage control and the reference DC-link voltage switchover control does not occur.

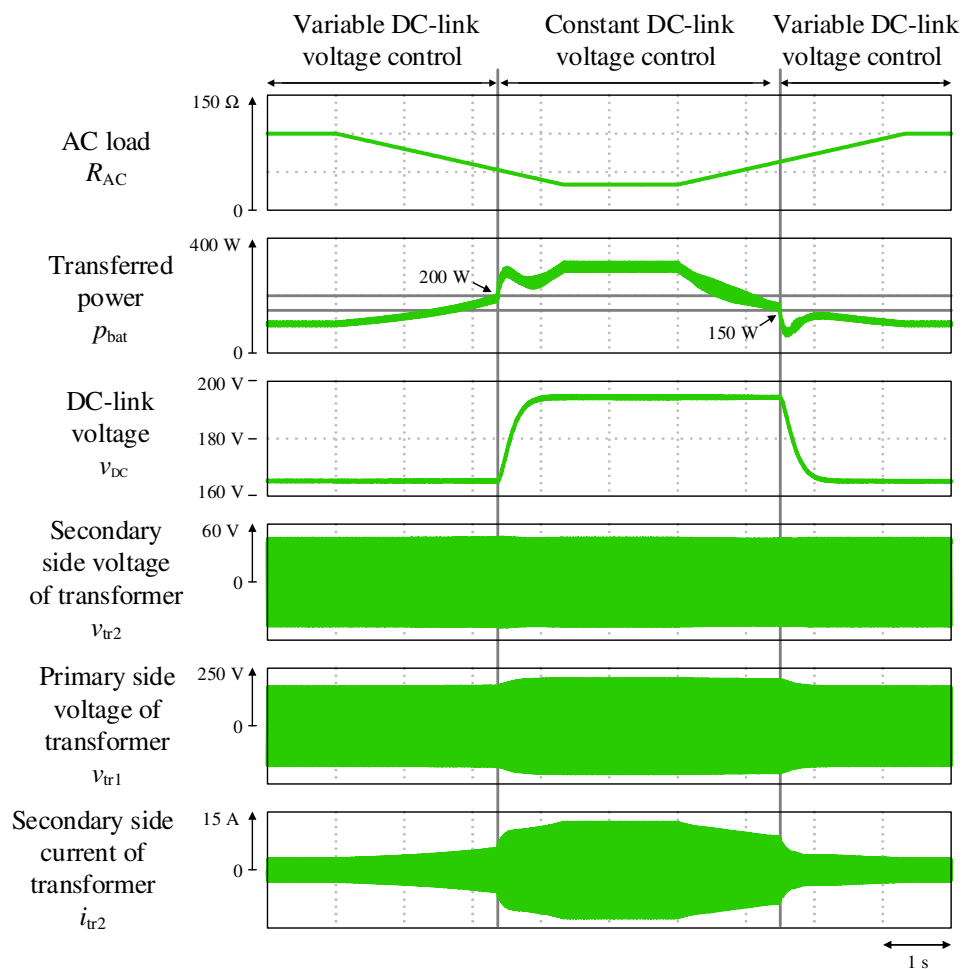


Figure 19. Simulation results for reference DC-link voltage switchover control.

6. Conclusions

In this paper, we deal with the variable DC-link voltage control of the DAB converter in a standalone WPGS for high-efficiency battery-discharging operation. Variable DC-link voltage control has been proposed to improve the power conversion efficiency under a light load. The DC-link voltage in the proposed control changes with battery voltage fluctuation. As a result, the peak value of the transformer current is suppressed, and the power conversion efficiency can be improved under a light load. Simulation results demonstrate that the proposed variable DC-link voltage control is highly efficient below 30% of the rated power of the DAB converter, and the constant DC-link voltage control is highly efficient over 40% of the rated power of the DAB converter. In addition, a reference DC-link voltage switchover control has been proposed to enable a high-efficiency drive under all load ranges. The reference DC-link voltage is switched over between the variable and constant depending on the transferred power of the DAB converter. The simulation results demonstrate that the reference DC-link voltage switchover control can operate properly. The power loss can be reduced under the light load by the proposed control. Thus, the validity of the proposed variable DC-link voltage control was confirmed.

Author Contributions: Y.T. significantly contributed to the design of the proposed control strategy and contributed to the implementation of digital computer simulations and experiments. H.Y. proposed the basic control topology and helped with the writing of this paper. All authors have read and agreed to the published version of the manuscript.

Funding: This research was funded by the Japan Power Academy.

Acknowledgments: This study was supported by a research grant from the Japan Power Academy.

Conflicts of Interest: The authors declare no conflict of interest.

References

1. Wu, Q.; Solanas, J.I.B.; Zhao, H.; Kocewiak, L.H. Wind Power Plant Voltage Control Optimization with Embedded Application of Wind Turbines and STATCOM. In Proceedings of the Asian Conference on Energy, Power and Transportation Electrification (ACEPT), Singapore, 25–27 October 2016; p. 16585658.
2. Ge, W.; Chen, H.; Liu, Q.; Tan, H.; Shen, L.; Wang, S.; Ji, Y. Optimization of wind power grid connection in multi-source and multi-region power generation system based on peak adjustment margin. In Proceedings of the Ninth International Conference on Intelligent Control and Information Processing (ICICIP), Wanzhou, China, 9–11 November 2018; p. 18401969.
3. Toledo, S.; Maqueda, E.; Rivera, M.; Gregor, R.; Wheeler, P.; Romero, C. Improved Predictive Control in Multi-Modular Matrix Converter for Six-Phase Generation Systems. *Energies* **2020**, *13*, 2660. [[CrossRef](#)]
4. Huu, D.N. A Novel Adaptive Control Approach Based on Available Headroom of the VSC-HVDC for Enhancement of the AC Voltage Stability. *Energies* **2021**, *14*, 3222. [[CrossRef](#)]
5. Saboori, H.; Jadid, S.; Savaghebi, M. Spatiotemporal and Power–Energy Scheduling of Mobile Battery Storage for Mitigating Wind and Solar Energy Curtailment in Distribution Networks. *Energies* **2021**, *14*, 4853. [[CrossRef](#)]
6. Global Wind Energy Council, Global Wind Energy Outlook 2016. Available online: <http://gwec.net/publications/global-wind-energy-outlook/global-wind-energy-outlook-2016/> (accessed on 30 June 2019)
7. Koutroulis, E.; Kalaitzakis, K. Design of a Maximum Power Tracking System for Wind-Energy-Conversion Applications. *IEEE Trans. Ind. Electron.* **2006**, *53*, 486–494. [[CrossRef](#)]
8. Taniguchi, D.; Narisada, Y.; Yamada, H.; Tanaka, T.; Tamura, T.; Yamada, S.; Okamoto, M. Variable Tip Speed Ratio Control in a Stand-Alone Small-Scale Wind Power Generation System. *J. Jpn. Inst. Power Electron.* **2017**, *43*, 43–49.
9. Lachguer, N.; Lamchich, M.T. Control Strategy of Permanent Magnet Synchronous Generator for Stand Alone Wind Power Generation System. In Proceedings of the International Aegean Conference on Electrical Machines and Power Electronics and Electromotion, Istanbul, Turkey, 8–10 September 2011; pp. 392–397.
10. Tian, C.; Zhang, C.; Li, K.; Chu, X.; Cui, N.; Wang, J. Control Strategy for Bi-Directional DC/DC Converter of a Stand-Alone Wind Power System. In Proceedings of the 3rd IEEE International Symposium on Power Electronics for Distributed Generation Systems, Aalborg, Denmark, 25–28 June 2012; pp. 297–300.
11. Takayama, Y.; Yamada, H. Dual Active Bridge Converter Based Battery Charger in Stand-Alone Wind Power Generation System with High-Inertia Wind Turbine. In Proceedings of the 22nd International Conference on Electrical Machines and Systems (ICEMS2019), Harbin, China, 11–14 August 2019; p. 1570545226.
12. Kheraluwala, M.N.; Gascoigne, R.W.; Divan, D.M.; Baumann, E.D. Performance Characterization of a High-Power Dual Active Bridge dc-to-dc Converter. *IEEE Trans. Ind. Appl.* **1992**, *28*, 1294–1301. [[CrossRef](#)]
13. Xue, L.; Shen, Z.; Boroyevich, D.; Mattavelli, P.; Diaz, D. Dual Active Bridge-Based Battery Charger for Plug-In Hybrid Electric Vehicle with Charging Current Containing Low Frequency Ripple. *IEEE Trans. Power Electron.* **2015**, *30*, 7299–7307. [[CrossRef](#)]
14. Yamanaka, H.; Yamada, H. Dual Active Bridge DC-DC Converter Based Wide Dimming Range LED Driver With High-Speed Turn-Off for High-Brightness LED Floodlight. *IEEJ J. Ind. Appl.* **2019**, *8*, 556–557. [[CrossRef](#)]
15. Malek, M.H.A.B.A.; Kakigano, H.; Takaba, K. Dual Active Bridge DC-DC Converter with Tunable Dual Pulse-Width Modulation for Complete Zero Voltage Switching Operation. *IEEJ Ind. Appl.* **2019**, *8*, 98–107. [[CrossRef](#)]
16. Ríos, S.J.; Pagano, D.J.; Lucas, K.E. Bidirectional Power Sharing for DC Microgrid Enabled by Dual Active Bridge DC-DC Converter. *Energies* **2021**, *14*, 404. [[CrossRef](#)]
17. Gierczynski, M.; Grzesiak, L.M.; Kaszewski, A. A Dual Rising Edge Shift Algorithm for Eliminating the Transient DC-Bias Current in Transformer for a Dual Active Bridge Converter. *Energies* **2021**, *14*, 4264. [[CrossRef](#)]
18. Baddipadiga, B.P.; Ferdowsi, M. Dual Loop Control for Eliminating DC-Bias in a DC-DC Dual Active Bridge Converter. In Proceedings of the International Conference on Renewable Energy Research and Application (ICRERA), Milwaukee, WI, USA, 19–22 October 2014; p. 14867746.
19. Bhattacharjee, A.K.; Tayebi, S.M.; Batarseh, I. Fast Response Dual Active Bridge Converter with Elimination of Transient DC Offset by Intermediate Asymmetric Modulation. In Proceedings of the IEEE Energy Conversion Congress and Exposition (ECCE), Portland, OR, USA, 23–27 September 2018; p. 18307624.
20. Takayama, Y.; Yamada, H. Power Loss Reduction by Stand-Alone Wind Power Generation System with Dual Active Bridge Converter Based Battery Charger. In Proceedings of the 21st IEEE Hiroshima section student symposium (HISS), Hiroshima, Japan, 30 September–1 October 2019; pp. 265–268.
21. Takayama, Y.; Yamada, H. Experimental Verification of Dual Active Bridge Converter Based Battery Charger in a Stand-Alone Wind Power Generation System. In Proceedings of the 23rd International Conference on Electrical Machines and Systems (ICEMS2020), Online, 24–27 November 2020; pp. 1022–1026.
22. Takeno, S. *Electrical Regulation and Plant Maintenance*; Tokyo Denki University Press: Tokyo, Japan, 2019.